Article

Regioselective Alkyne Cyclotrimerization with an In Situ-Generated [Fe(II)H(salen)]·Bpin Catalyst

Cei Benjamin Provis-Evans, Samantha Lau, Vera Krewald, and Ruth L Webster

ACS Catal., **Just Accepted Manuscript** • DOI: 10.1021/acscatal.0c03068 • Publication Date (Web): 07 Aug 2020

Regioselective Alkyne Cyclotrimerization with an *In Situ*-Generated [Fe(II)H(salen)]·Bpin Catalyst

Cei B. Provis-Evans,† Samantha Lau,† Vera Krewald,*,‡ and Ruth L. Webster*,†

†Department of Chemistry, University of Bath, Claverton Down, Bath BA2 7AY, United Kingdom

‡Department of Chemistry, Theoretical Chemistry, TU Darmstadt, Alarich-Weiss-St. 4, 64287 Darmstadt, Germany

ABSTRACT: A mild, efficient and regiospecific catalytic cyclotrimerization of alkynes to form 1,2,4-substituted arenes has been discovered. From a cheap and air-stable [Fe(salen)]$_2$-μ-oxo complex and readily available pinacol borane (HBpin), a monomeric [FeH(salen)]·Bpin species formed *in situ* acts as the active catalyst. This species is shown to feature a hemilabile salen ligand stabilized via interactions with the boron entity. The formation, identity and reaction mechanism of the active species is supported by complementary kinetic, spectroscopic and computational data. The active catalyst undergoes hydrometallation of a coordinated alkyne to form a vinyl iron species, stepwise additions of two more alkynes across the Fe-C bond to form a pendant triene, which upon ring-closure forms the arene product. The catalytic cycle is closed by substitution of the product with alkyne substrate. With the active [FeH(salen)]·Bpin catalyst, atom-efficient, intermolecular trimerization is shown with high regioselectivity for a diverse range of substrate substitution patterns and presence of functional groups.

KEYWORDS iron, homogeneous catalysis, reaction mechanisms, density functional theory, salen ligands, cyclotrimerization

1. INRODUCTION

The cyclotrimerization of alkynes remains one of the most atom-efficient ways to prepare benzene rings.[1,2] Since benzene motifs are ubiquitous in organic chemistry,[3] cyclotrimerisation reactions have wide-ranging application potential including liquid crystals,[4] light-emitting molecules,[5] natural products,[6–9] and pharmaceuticals.[10–12] The reaction of three molecules of acetylene to form benzene was first discovered in the mid-19th century by Bertholet using high temperatures and pressures.[13] In 1948, Reppe *et al.* found a practical catalytic route to trimerize propargyl alcohols at much lower temperatures and ambient pressure.[14] While today a diverse range of catalytic procedures is available in which polymeric and oligomeric side-products are minimized,[15,16] challenges remain: many of the catalysts used in these syntheses require scarce and expensive platinum group metals or relatively harsh conditions and many are not regioselective.

If a terminal alkyne is trimerized, it can form two distinct regioisomers with 1,3,5- or 1,2,4-substitution patterns. Often, the only way of controlling this is to use steric factors or cleverly tethered di-alkyne substrates to allow the preferential formation of one isomer, as exemplified by Deiters' ruthenium catalyst (Scheme 1a).[8] While effective, this approach perhaps moderates the appealing atom efficiency of the transformation, even if using earth-abundant catalysts.[17–19]

Scheme 1. Previous cyclotrimerizations (1a-c), this work (d) and structure of 1.

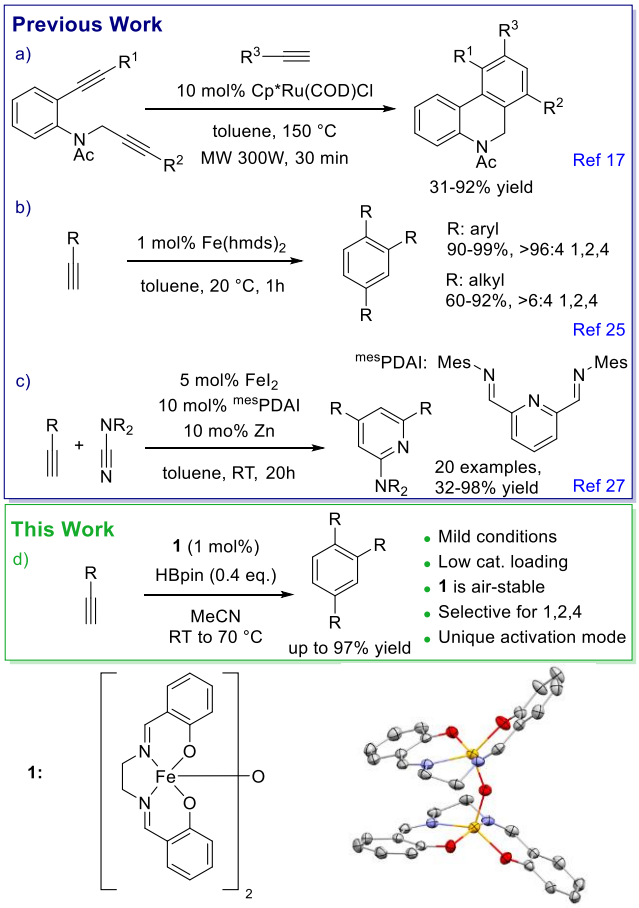

Transition metal complexes featuring the salen (salen = *N,N'*-bis(salicylidene)ethane-1,2-diamine) ligand are excellent catalysts for a range of transformations, one notable example being enantioselective epoxidations mediated by Jacobsen's catalyst.[20] Our past work with iron(salen) complexes explored hydrophosphination chemistry using an $[Fe(salen)]_2$-μ-oxo pre-catalyst in which the iron ions have distorted square-pyramidal ligand spheres.[21] During the course of these studies it became apparent that the pentacoordinate iron center would need an activation event in order to develop catalysis beyond hydrophosphination. Notably, studies by Hilt have shown that simple Fe(salen) complexes can be reduced by Zn to allow for epoxide ring expansion (and thus C-C bond formation).[22] With this in mind we sought to expand the reactivity of the $[Fe(salen)]_2$-μ-oxo pre-catalyst to effect the cyclotrimerization of alkynes to form (poly)cyclic molecules under mild conditions.

Advances in the field of iron catalyzed cyclotrimerization have brought regioselective processes that have mitigated the requirement for expensive reagents. An example is the highly active $Fe(hmds)_2$ catalyzed trimerization system formulated by Jacobi von Wangelin and co-workers (Scheme 1b),[23] which proceeds via a substrate-induced reduction of the pre-catalyst to generate catalytically active nanoparticulate iron. During the preparation of this manuscript, Jacobi von Wangelin reported dual organo-photoredox/$FeCl_2$-mediated catalysis which is also nanoparticulate in nature.[24]

The benefit of using a discrete, ligated homogeneous iron catalyst lies in the tunability of the metal center. By anchoring a molecular catalyst to a surface the advantages of the heterogeneous and homogeneous world can be combined: a tunable catalyst that is easily separated from the products. Examples of homogeneous iron-catalyzed intermolecular alkyne cyclotrimerization include trimerization of acetylene from McGuinness, although no other alkynes were tested,[25] an Fe(0) *N*-heterocyclic carbene (NHC) catalyst from Deng with low to moderate regioselectivity,[26] an Fe N,N,N-chelate from Gunanathan which operate for a wide range of substrates,[27] while Louie and coworkers have reacted untethered alkynes with cyanamides to form a wide variety of 2,4,6-substituted pyridines using FeI_2 in combination with a ^{mes}PDAI ligand and catalytic Zn (Scheme 1c).[28]

We show below that the salen ligand undergoes an unusual conformational change to form the active catalyst. In the vast majority of cases, ranging from coordination chemistry, catalyst design and implementation[29,30] to artificial metalloenzyme studies,[31,32] the salen ligand maintains a rigid, tetracoordinate, approximately square-planar geometry around the metal center.[33–37] Exceptions can be found when the *N,N'*-backbone contains a chain of three or more carbons, which allows the ligand to twist such that both axial and equatorial ligand coordination is observed at the metal center. To the best of our knowledge, however, there are no examples where the salen ligand exhibits lability or hemilability during catalysis. In fact, its stability as a tetracoordinate spectator ligand is one of the reasons why it features so prolifically in the literature.

Herein, we report the use of a simple $[Fe(salen)]_2$-μ-oxo pre-catalyst (**1**, Scheme 1) and pinacol borane (HBpin) co-catalyst for the efficient and selective cyclotrimerization of alkynes. We show that HBpin serves a dual role: not only as a reducing agent, but also in forming the catalytically active complex itself. This second role provides a unique example of salen hemilability via one of the phenoxy arms, resulting in the formation of an active [Fe(II)H(salen)]·Bpin species (**5**). In the catalytically active complex, the iron center is ligated by an unprecedented twisted salen coordination environment. Our findings are supported by comprehensive experimental and computational investigations.

2. RESULTS AND DISCUSSION

2.1 Optimization and Substrate Scope

Preliminary reactions in MeCN (Table 1, entry 1) show quantitative conversion of phenylacetylene (**2a**) to a mixture of 1,3,5- and 1,2,4-triphenylbenzene (**3a**, 2:98 respectively) after 2 h with 1 eq. of HBpin and 5 mol% of **1**. Reducing the catalyst loading to 1 mol% and the reaction time to 1 h gives the same conversion (entry 2). Solubility of **1** limits the solvent choice; Et_2O and solvent-free conditions give poor conversion and low isolated yield due to a protracted work-up procedure being necessary (compare entry 2 to entries 3 and 4). To elucidate the role of HBpin, a wide variety of reducing agents were tested (entries 5 to 15). None achieve any conversion to the cyclotrimer, showing clearly that the speciation of the borane is important for reactivity. Similarly, the $[Fe(salen)]_2$-μ-oxo pre-catalyst is essential since reactions testing simple iron salts $FeCl_2$ and $FeCl_3$ instead of **1** show no activity (SI, Section 3).

Having ascertained that HBpin and the $[Fe(salen)]_2$-μ-oxo pre-catalyst are necessary reactants, the loading of HBpin required for full conversion was studied. With 0.02 eq. and 0.1 eq. HBpin, no conversion to cyclotrimer is observed (entries 16 and 17) while loadings of 0.3 eq. and 0.4 eq. afford almost quantitative yields (entries 19 and 20). These non-linear results suggest that not only is HBpin the only reducing agent tested which demonstrates any activity, it is also acting in a co-catalytic manner. These findings invite speculation as to its specific role or roles within the catalytic cycle.

Table 1: Optimization of reaction conditions.

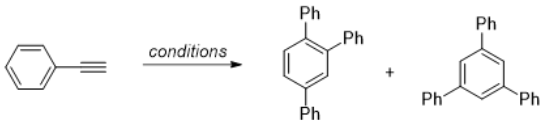

2a **3a**

Entry	Solvent	Reductant	Total conversion (yield) (%)[b]
1[a]	MeCN	HBpin (1 eq)	100
2	MeCN	HBpin (1 eq)	100 (97)
3	Et_2O	HBpin (1 eq)	68 (15)
4	Neat	HBpin (1 eq)	70 (27)
5[c]	MeCN	Ascorbic. acid (1 eq)	(0)
6[c]	MeCN	Na ascorbate (1 eq)	(0)
7	MeCN	Zn dust (1 eq)	(0)
8[c]	MeCN	Mg (1 eq)	(0)

9[c]	MeCN	Mn (1 eq)	(0)
10[c]	MeCN	CH_2O (1 eq)	(0)
11[c]	MeCN	TMDS[d] (1 eq)	(0)
12[c]	MeCN	PMHS[e] (1 eq)	(0)
13[c]	MeCN	$NaBH_4$ (1 eq)	(0)
14[c]	MeCN	$NaBH_4$ + MeOH (1 eq)	(0)
15	MeCN	$NaBH_4$ (1 eq)	(0)
16	MeCN	HBpin (0.02 eq)	(0)
17	MeCN	HBpin (0.1 eq)	(0)
18	MeCN	HBpin (0.2 eq)	(13)
19	MeCN	HBpin (0.3 eq)	(90)
20[f]	MeCN	HBpin (0.4 eq)	(97)

Conditions: **2a** (0.25 mmol), **1** (1 mol%), inert atmosphere, RT, 1 h. [a] 5 mol% **1**, 2 h. [b] Spectroscopic conversion to **3a** measured by ^{1}H NMR against an internal standard/isolated yield of both regioisomers. [c] **2a** (0.25 mmol), **1** (1 mol%), RT, 1 h. [d] Tetramethyldisiloxane. [e] Polymethylhydrosiloxane. [f] Obtained as a 98:2 ratio of 1,2,4-triphenylbenzene: 1,3,5-triphenylbenzene.

With optimized conditions in hand (Table 1, entry 20), the scope of the transformation was explored (Scheme 2). For all aryl terminal alkynes tested, we find rapid conversion, good to excellent yields and excellent selectivity for the 1,2,4-regioisomer (**3a**-**h**). The presence of a variety of substitution patterns do not appear to substantially impact yield or selectivity (**3c**, **3d**, **3e**, **3g**), although the presence of bulky substituents does impact the speed at which full conversion is achieved (**3b**). The presence of labile amine protons (**2f**) consumes HBpin to form N-B bonds[38] before trimerization takes place. However, this can be mitigated by using additional HBpin to form R-N(Bpin)$_2$ which can then be trimerized. In addition to aryl alkynes, the methodology is suitable for trimerizing ethyl propiolate (**2i**) with excellent selectivity for the 1,2,4-regioisomer in a very good isolated yield.

It also proved possible to cyclotrimerize terminal aliphatic alkynes, albeit under more forcing conditions, with the reaction of 1-heptyne yielding 72% **3j** after 20 h at 70 °C. However, unlike **3a** to **3i**, this material shows an equal split between the 1,2,4- and 1,3,5-regioisomers. This is also the case for 1-pentyne and benzyl acetylene (**2k**, **2l**). No trimerization was detected for cyclopentyl acetylene or benzonitrile (**2n**, **2o**), while ill-defined reactivity is observed for the silyl alkyne **2m**. The internal alkyne diphenylacetylene **2p** forms an intractable mixture, highlighting the challenges of cyclotrimerizing internal alkynes. Previous examples of Fe-catalyzed trimerization of internal alkynes are limited. For instance, Tilley's two-coordinate Fe(I)NHC species achieves quantitative yields of hexamethylbenzene from 2-butyne after 3 h at RT.[39]

Scheme 2. Optimized 'standard' conditions for alkyne cyclotrimerization, and substrate scope.

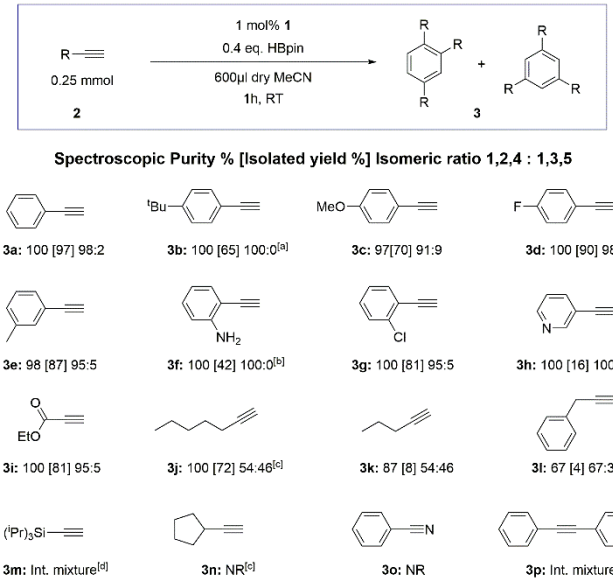

[a] 20 h. [b] 3 eq. HBpin (2 eq. consumed in forming R-N(Bpin)$_2$). [c] 20 h, 70 °C. [d] Intractable mixture of new aromatic signals observed in ^{1}H NMR spectra. NR: no reaction detected.

2.2 Kinetics

Bearing in mind that HBpin is mandatory for catalysis, the nature of the active catalytic species and the mechanism by which the reaction proceeds were investigated. The possibility of a radical mechanism was probed by using a radical clock ((chloromethyl)cyclopropane).[40] For an intermolecular radical mediated mechanism, the ring-opening formation of butene and concurrent retardation of the catalysis would be expected; neither are observed over the same time period (SI, Section 3).

To determine whether nanoparticles are responsible for catalysis, a substoichiometric amount of catalyst poison (PMe_3) was used. This should completely stop catalysis occurring on the surface of nanoparticles, while only inhibiting (by a factor related to the excess of catalyst over poison) catalysis occurring in solution. Upon addition of 0.5 eq. of PMe_3 vs. **1** the reaction still proceeds, albeit with a reduced isolated yield of 46% after 18 h at RT (cf. Table 1, entry 20). This finding supports a homogeneous rather than a nanoparticulate mechanism.[41]

In order to probe the reaction in more depth, the consumption of alkyne was tracked using *in situ* ^{1}H NMR spectroscopy (SI- Fig. S1). **2b** was used as our standard substrate for the following studies because it reacts slower than **2a**, with less data lost in the ~15 min between reaction start and the collection of the first spectrum. The reaction profile shows a ~30 minute induction phase and sigmoidal shape (Fig. 1, ●), which is somewhat reminiscent of a nanoparticulate catalyzed reaction.[42] Therefore, a further catalyst poisoning experiment was conducted with PMe_3 in the same way as noted previously but tracked over time (Fig. 1, ■). This experiment shows an initial lag phase as per the poison-free reaction, followed by the relatively fast conversion of about 30% of the starting material **2b** before the conversion slows at around ~62 min. Slow conversion continues until 43% of **2b** is consumed after 412 min. That the reaction

demonstrably continues in the presence of PMe_3 is further evidence against a nanoparticle mediated mechanism, despite the sigmoidal shape of the poison-free reaction profile.

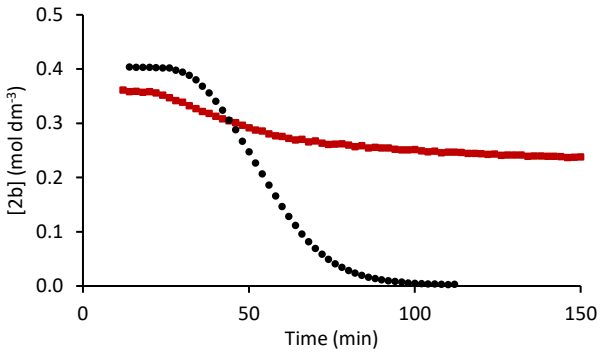

Figure 1. Concentration of **2b** over time under standard conditions (●) and with PMe_3 additive (■), calculated by ^1H NMR spectroscopy against 1,3,5-trimethoxybenzene (TMB) internal standard.

Another argument against a nanoparticulate mechanism is that no cyclotrimerization is observed with any reducing agent but HBpin, including those with similar reducing power to HBpin. It is unlikely that HBpin would be unique among the reducing agents tested in its ability to form nanoparticles from the pre-catalyst, and therefore it must be another aspect of HBpin and its interaction with iron which allows the catalysis to proceed.

The ~30-minute delay with no notable activity followed by rapid conversion suggests that there is a period of catalyst activation. A stoichiometric reaction of the burgundy colored pre-catalyst **1** and HBpin gives an auburn colored solution and shows H_2 production (^1H NMR) and new peaks in the ^{11}B NMR spectrum corresponding to pinBOBpin (Fig. S16, S17). This, coupled with the 30-minute activation period, could indicate a reductive activation mechanism, whereby HBpin reduces the Fe(III) centers of **1** to Fe(II), while concurrently splitting the dimer and appropriating the μ-oxygen to form a new pinBOBpin species (Scheme 3).

Scheme 3. Plausible mechanism for reduction of Fe(III) dimer (1) pre-catalyst to Fe(II) monomer (4) by HBpin.

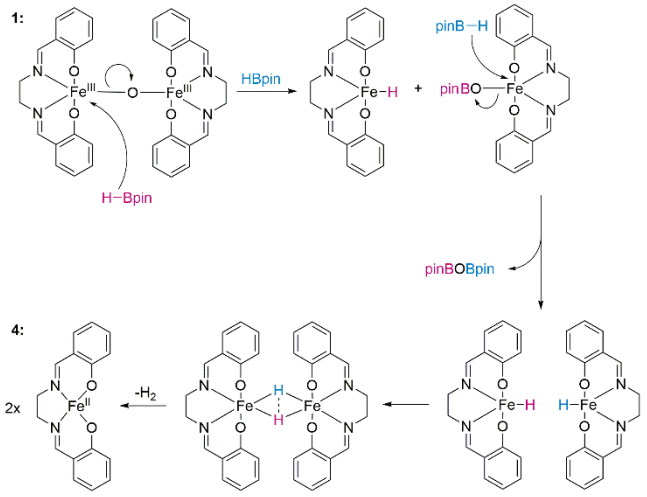

If catalyst activation involves formation of a monomeric species such as **4**, the reaction would demonstrate 0.5 order kinetics with respect to **1**. Reaction profiles of the transformation of **2b** at five loadings of **1** using standard conditions were collected using *in situ* ^1H NMR spectroscopy. The rates of consumption of **2b** were calculated from the linear conversion phase of the reaction (~30-60 min) to determine the order with respect to **1** (SI, Section 6). The plot of rate vs. $[\mathbf{1}]^{0.5}$ (Fig. 2) has an R^2 value of 0.997, showing conclusively that the reaction is 0.5 order in **1**, i.e. 1st order in monomeric iron species.

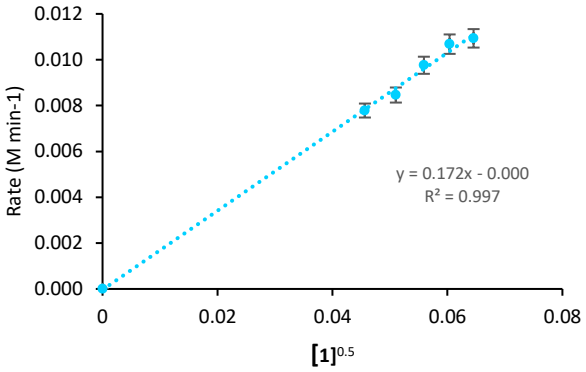

Figure 2. $[\mathbf{1}]^{0.5}$ vs rate. R^2 of line through origin > 0.995, therefore reaction 0.5 order with respect to the dimeric pre-catalyst.

2.3 Identity of the Active Species

If the monomeric Fe(II) complex **4** is the active species, the role of HBpin would be simply to reductively split the dimeric pre-catalyst **1**, and therefore **4** should itself be competent in catalysis. To investigate the catalytic capacity of **4**, it was synthesized independently under inert conditions using an electrochemical set-up with a sacrificial iron anode. **4** is isolated as a lilac solid (SI, Section 4, No. 1). Using the obtained **4**, no cyclotrimerization was observed in the absence of HBpin (Scheme 4, reaction 1),[43] providing evidence that **4** alone is not the active catalytic species. However, the fact that cyclotrimerization rapidly occurs once HBpin is added (Scheme 4, Reaction 2) strongly suggests that **4** represents a related species, likely an intermediate between **1** and the active species. This, taken with the previous evidence for HBpin acting as a reducing agent, indicates a dual role for HBpin in this catalysis: (i) reductively splitting the μ-oxo dimer to form **4**, (ii) transforming **4** into the active catalyst in a second, as yet undefined reaction.

A plausible second role for HBpin might involve the formation of an Fe-H species.[44] Therefore, a RT stoichiometric reaction of **1** with 20 eq. of HBpin was conducted to detect any hydride signal. ^1H NMR analysis shows a candidate peak in the upfield region (-25 ppm, Fig. S18).[45,46] Repeating the reaction using DBpin does not show a peak at -25 ppm, strongly suggesting that an iron hydride is indeed forming as the catalytically active species (Fig. S19). Further support comes from the fact that high-spin, paramagnetic **1** is transformed into a diamagnetic complex upon addition of HBpin. This is evidenced by the appearance of aryl proton signals

during the activation step that are absent in the spectrum of pure **1** (Fig. S20, Fig. S21).

Thus, the experimental evidence can be confidently interpreted as follows: in the presence of HBpin, the iron dimer **1** is reductively split to form two eq. of monomeric **4**, which is catalytically inactive. After reacting a second time with HBpin, **4** forms a closed-shell Fe-H species which is catalytically competent for the cyclotrimerization of alkynes to 1,2,4-substituted arenes. The composition and properties of the active species are discussed in the following.

Scheme 4. Attempted trimerization using 4 with/without HBpin. 4 used at 2 mol% to give same quantity of Fe as 1 mol% of 1.

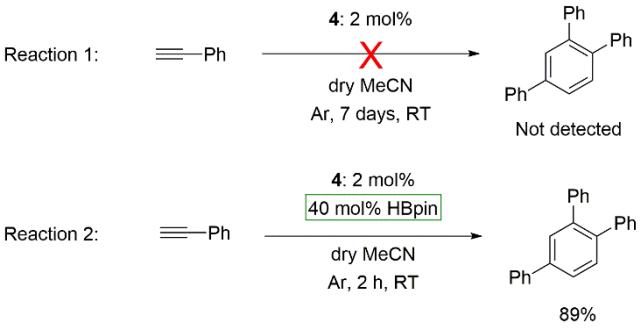

The catalyst activation mechanism proposed above was comprehensively modelled using density functional theory (DFT) to identify the geometries, electronic structures and properties of the catalytically relevant species. Using the BP density functional with a triple-ζ basis set and corrections for solvation, relativistic and dispersion effects (SI- Section 8), we formulated molecular models based on the experimental findings and calculated the relative free energies involved. This study ascertained that the HBpin-driven reductive splitting of **1** to **4** is an exergonic process (-18.8 kcal/mol, Scheme 5). **4** was found to be most stable with a triplet spin multiplicity. Because the NMR data showed that catalysis is driven by a closed-shell complex, this finding serves as additional confirmation that **4** cannot be the active species.

Scheme 5. Computed reaction path for the HBpin reduction of 1 to 4 with calculated Gibbs free energies (kcal/mol) for each step, and the predicted structure of an HBpin adduct of 4; 5. The structure of 5 is color-coded with Fe: orange, C: dark grey, H: light grey, N: blue, O: red, B: teal.

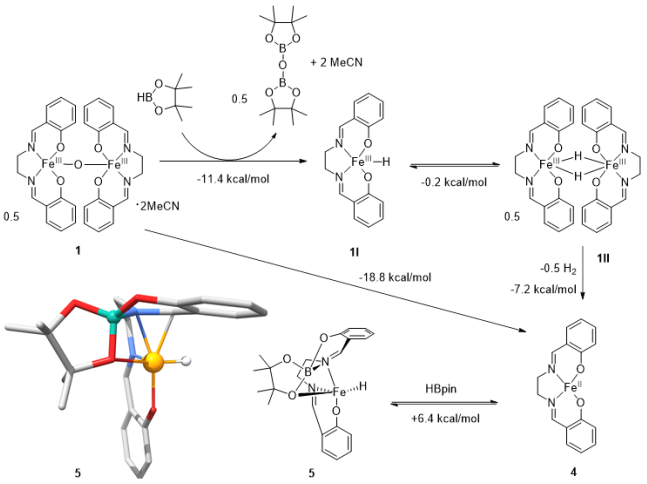

From an extensive search of plausible candidates for the active species, a closed shell intermediate was identified (**5**, Scheme 5), which credibly rationalizes the experimental observations while remaining energetically accessible (+6.4 kcal/mol). In **5**, the H from HBpin forms an iron hydride (Fe-H bond length: 1.48 Å) and the Bpin residue is incorporated into the complex through several interactions with the iron center and the salen ligand. One of the Bpin pinacol oxygen atoms binds to the iron ion (Fe-O distance: 2.51 Å). The salen ligand acts as a hemilabile ligand with one arm of the salen ligand decoordinated from iron and perpendicular to the other salen arm. This distortion is stabilized by a two newly formed bonds between the boron atom and the imine nitrogen and one of the phenolate oxygen atoms and so that in total a six-membered ring is formed. The imine nitrogen remains attached to the iron centre, forming a four-membered Fe-O-B-N ring perpendicular to the six-membered ring. Notably, the carbon adjacent to the imine nitrogen in the labile salen arm interacts with the iron. This is shown by the short Fe-C distance (2.09 Å) and the positioning of the C-bound hydrogen atom. Overall, the coordination geometry of boron is tetrahedral and that of iron is close to pseudo-square pyramidal with the open coordination site *trans* to the non-labile imine nitrogen.

The twisted conformation of the salen ligand appears to be unprecedented for a salen ligand with an ethylene diamine backbone. With a propylene backbone, a few examples of transition metal dimers and polymers with a twisted salen ligand are known. In contrast to complex **5** described here, however, the O,N,N,O-coordination mode is retained in these cases.[33,34]

Attempts to obtain X-ray quality crystals of **5** have been unsuccessful.[47] In agreement with the NMR evidence of a diamagnetic species forming, the triplet and quintet spin states of **5** are computed to have higher energies than the singlet state with a range of different hybrid density functionals (see SI- Section 8). We further note that the frontier MOs of **5** are dominated by iron d-orbital contributions that render a π-interaction with PMe_3 likely. The adduct **5**-PMe_3 is computed as stabilized by -16.0 kcal/mol, providing a rationale for the lowered yield in the PMe_3 poisoning experiment.

If there is a reaction between **4** and HBpin to form the active species, the formation of a complex akin to **5** should be independent of the identity of the substrate. This was tested by using **2a** instead of **2b** as the substrate, which is expected to give similar lag times (Fig. 3A). The lag phase observed for the cyclotrimerization of **2a** is around 25 min, comparable to that observed for **2b** (~30 min). This supports the assertion that the formation of the active species does not involve the substrate. Figure 3A also shows that the rate of **2a** conversion during the linear phase is slower than for **2b** (**2a**: 0.015 M min^{-1}, **2b**: 0.011 M min^{-1}**)**. This suggests that unlike the lag phase, the steric bulk of the substrate has an influence on the rate once the reaction is underway.

Confirmation that **5** is a hydride comes from a kinetic deuteration experiment using deuterated pinacol borane (DBpin, Fig. 3B). When using DBpin instead of HBpin, the lag time for catalyst activation doubles to ~60 min. This shows that changes in the lability of the B-H/D bond make a substantial difference to the speed of active species formation. In addition, the rate of **2a** consumption during the linear conversion phase is 0.005 M min^{-1} (Fig. 3B), giving a kinetic isotope effect (KIE) of 2.7 ± 0.2. This large positive KIE suggests that the rate-limiting step of the reaction involves formation or breaking of H/D-bonds, lending further support to the presence of Fe-H originating from HBpin in the active catalytic species. Finally, inspection of the ^{1}H NMR spectrum of the completed reaction shows no D incorporation in the 1,2,4-trimer product, supporting the assertion that the borane is acting in a purely catalytic manner.

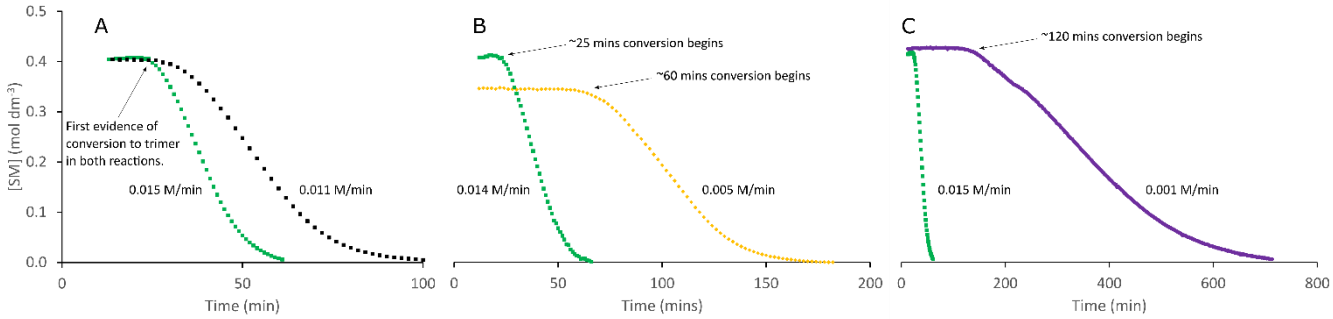

Figure 3. Reaction profiles conducted in CD_3CN, quantification by ^{1}H NMR vs. TMB internal standard. A: **2a** (■) and **2b** (■) trimerizations with **1** under standard conditions. B: **2a** trimerization with **1** using HBpin (■) and DBpin (◆), both added as 1.35 M solutions in benzene. C: Profile of **2a** trimerizations in CD_3CN using **6** (●) and **1** (■) as catalysts. Rates shown are for the linear conversion phase of the reactions.

Since **5** was predicted purely computationally, we sought experimental support for its highly twisted salen conformation. Much of the salen distortion seen involves rotation around the imine such that the aryl groups become much more perpendicular to each other than in **1**. This distortion can be quantified by measuring the angle between planes drawn from the two *ipso*-carbons on the respective rings, with the angle averaged for dimers (SI- Section 7 for examples, Section 8 for full set of geometries). The average ligand distortion of **1** is 11°, while in **5** it is 69°. An attempt was made to force minimal distortion through a ligand modification that uses a rigidly planar phenyl backbone (**6**, Fig. 4) which shows an average ligand distortion of 6° (SI- Section 4). This more rigid ligand should resist distortion more effectively, and therefore **6** would impede the formation of the active species and result in a slowing of catalysis.

Indeed, cyclotrimerization using **6** is slower (Fig. 3C): the lag phase is ~120 min, while the rate of conversion of **2a** is 0.001 M min^{-1}. The elongated lag phase using a rigid ligand implies an energetically more demanding activation step, supporting the postulation that ligand distortion is part of the active species formation. The lower rate of reaction also supports this. It is likely that due to the more challenging formation of the active species, a smaller proportion of the iron resides in an active state, which thereby slows the reaction. Although we cannot disentangle the electronic and steric effects of the ligand modification, it appears likely that the steric effect will be dominant.

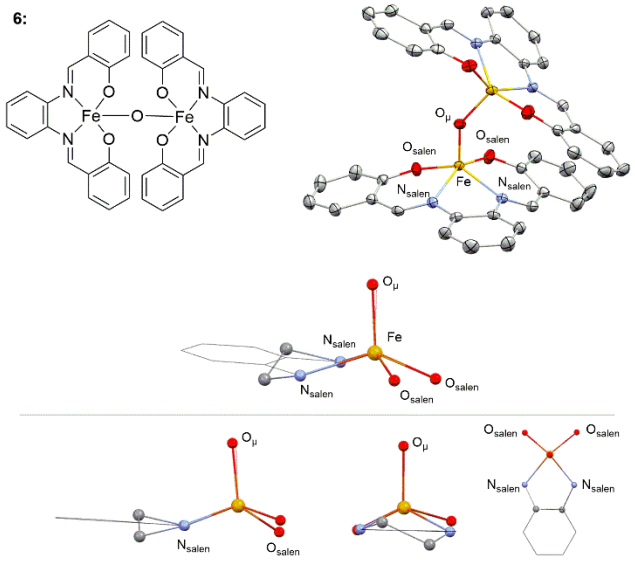

Figure 4. Top: complex **6**, with phenyl backbone, planar nature of ligand shown in crystal structure. Bottom: wireframe of **6** overlaid with **1** shown along different axes to demonstrate the planarity of **6**.

Further spectroscopic support was sought for the existence of **5**. Fig. 5 shows good agreement between experimental

and TDDFT-computed UV-Vis spectra of **4** (SI, Section 4, No. 2). Note that the stabilization of all species through interaction with the acetonitrile solvent was tested routinely. For **4**, the computed spectrum is based on a structure with one explicit acetonitrile molecule (see inset). A UV-Vis spectrum of **1** with 10 eq. HBpin in dry MeCN under inert conditions was collected and compared to the predicted spectrum of **5** (Fig. 5). Again, good agreement between experiment and prediction is found.

The experimentally obtained UV-Vis spectrum of the reaction of **1** with HBpin shows two maxima between 450-520 nm, for which corresponding transitions are found in the computed spectrum of **5** (Fig. 5). The computed difference densities show that the intense transition at 455 nm has metal-to-hydride charge transfer character; here and in the lower-energy transition, density is shifted from iron to the B-bound nitrogen atom (inset in Fig. 5). This further supports an Fe-H fragment and Bpin in close proximity to iron in the active species. Overall, the spectral differences between **4** and **5** and the computational interpretation provide strong evidence for the formation of a species possessing the geometric and electronic structure of **5** or a very similar species.

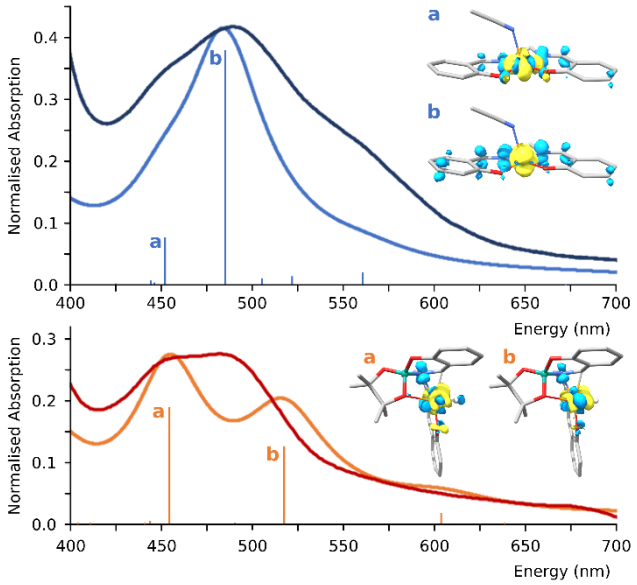

Figure 5. Top: UV-Vis spectra of **4** in MeCN (experiment: dark blue, calculation: light blue). Bottom: experimental spectrum of **1** + 10 eq. HBpin after 20 min (red trace, maxima at 452 and 490 nm) and predicted UV-Vis spectrum of **5** (orange trace, maxima at 455 and 517 nm). Vertical lines show individual calculated transitions which are broadened to obtain the line spectra; intensities of the calculated spectra are scaled to the maxima of the experimental spectra. The insets show the difference densities associated with the most intense transitions (yellow: density loss; light blue: density gain; contour value: 0.0035).

2.4 Catalytic Mechanism

Initially, a catalytic cycle starting from **4** was evaluated computationally (Scheme S1). Although the relevant intermediates are found and a catalytic cycle can be constructed, a prohibitively endergonic second alkyne addition step (ΔG= +24.8 kcal/mol) was found that could not be mitigated. This finding is likely reflective of the more congested iron environment in **4** relative to **5**, and is fully consistent with the experiment showing that **4** is unable to catalyze the cyclotrimerization without addition of HBpin.

Given the spectroscopic and kinetic evidence presented for an active catalytic species like **5**, this was used as a starting point for a more thorough computational evaluation of the catalytic cycle. The mechanism developed here provides explanations for the strong 1,2,4-selectivity with aryl alkynes and propiolates, and the reasons this selectivity diminishes for alkyl and benzyl alkynes.

Scheme 6 outlines the key steps of the reaction based on a preliminary catalytic cycle (Scheme S2). This scheme does not yet provide an explanation for the observed regioselectivity, the elucidation of which is the primary objective of the mechanistic study below.

Scheme 6. Summary of major steps in the proposed catalytic cycle.

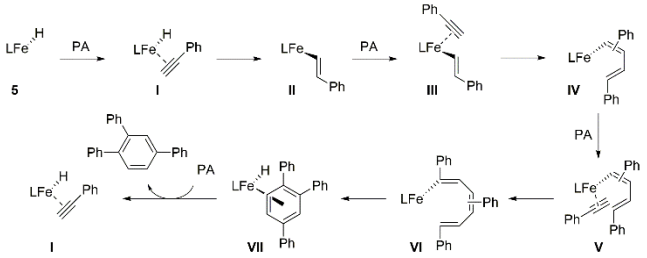

Since understanding the orientation of each alkyne molecule at the point of coordination and insertion into the growing alkene chain is vital to understanding the regiochemistry of the product, an exhaustive set of reaction pathways was explored with phenylacetylene as the model substrate. All plausible orientations of the catalytic species at each stage of the catalytic cycle were targeted (Fig. 6). We note that several recurring types of transition state, such as coordination, rotation around a bond or the formation of H-bonds, are expected to have low barriers and will not be rate-determining. Note also that in the following the label **5** is dropped in favor of referring to the individual intermediates with roman numerals for clarity.

Beginning from the top of Fig. 6, the two possible orientations of a single alkyne coordinating to **5** are shown; $\mathbf{I_A}$ and $\mathbf{I_B}$. All species were optimized with singlet spin multiplicity since this is the lowest energy electronic structure solution for **5**. $\mathbf{I_A}$ and $\mathbf{I_B}$ are assumed to be in equilibrium as the alkyne will be free to rotate. A hydrometallation step to form an Fe-vinyl species can proceed from either of these. Attempts to converge the forward-facing Markovnikov substituted species $\mathbf{II_{BA}}$ and $\mathbf{II_{BB}}$ from $\mathbf{I_B}$ failed, showing that neither are stable intermediates and thus allowing us to discount these routes. Similarly, a backwards facing version of a Markovnikov substituted species $\mathbf{II_{BC}}$ can be excluded based on the experimental observation that no deuteration occurred on the product when DBpin was used. If this route were viable, H/D scrambling would be observed as the

terminal H/D atoms of the vinyl species would be equally likely to be included in the product.

Therefore, catalysis must proceed from $\mathbf{I_A}$ by hydrometallation through **TS($\mathbf{I_A}$,$\mathbf{II_{AA}}$)** to the forward pointing Fe-vinyl species $\mathbf{II_{AA}}$. This vinyl can rotate and shift backwards to form $\mathbf{II_{AB}}$, which is energetically preferred (-6.3 kcal/mol). $\mathbf{II_{AA}}$ and $\mathbf{II_{AB}}$ can both coordinate a second alkyne molecule with the phenyl group oriented either away from or towards the alkene, affording four intermediates: $\mathbf{III_{AAA}}$, $\mathbf{III_{AAB}}$, $\mathbf{III_{ABA}}$ and $\mathbf{III_{ABB}}$. Next, the activated alkyne inserts into the Fe-C bond of the vinyl species to form four σ-bound diene species ($\mathbf{IV_{AAA}}$, $\mathbf{IV_{AAB}}$, $\mathbf{IV_{ABA}}$ and $\mathbf{IV_{ABB}}$).

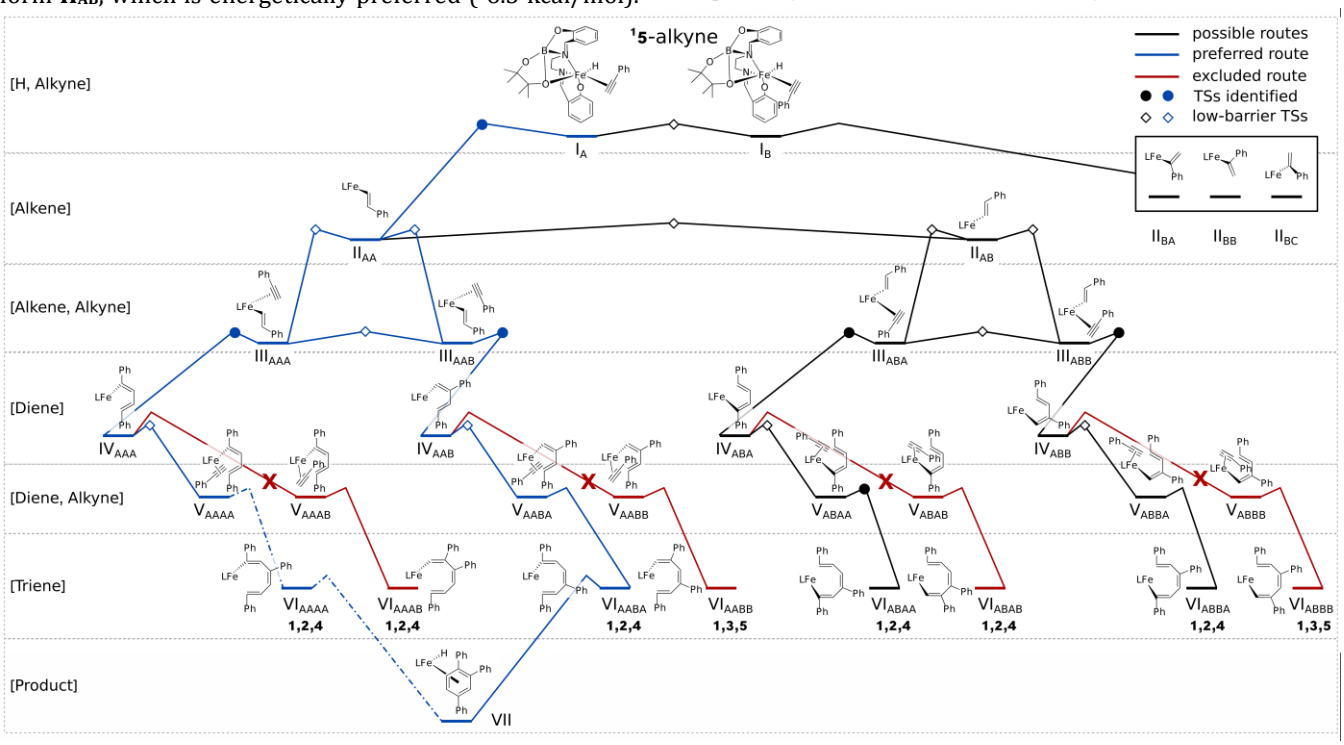

Figure 6. Computed reaction pathways for the trimerization of **2a**; note that the steps are not drawn on an energy scale. Seven distinct intermediate conformations around iron are considered: I: Fe-hydride with a π-bound alkyne; II: σ-bound alkene; III: σ-bound alkene with a π-bound alkyne; IV: σ-bound diene; V: σ-bound diene with a π-bound alkyne; VI: σ-bound triene; VII: π-bound benzene. The σ-bound alkenes are assumed to freely rotate. Gibbs free energies for the favored path are shown in Scheme 7 and in the SI for all species.

Reaction paths through **TS($\mathbf{III_{AAA}}$,$\mathbf{IV_{AAA}}$)** and **TS($\mathbf{III_{AAB}}$,$\mathbf{IV_{AAB}}$)** involve low-energy barriers with values that lie within the error of the computational method used (-1.3 and -0.3 kcal/mol respectively). In contrast, **TS($\mathbf{III_{ABA}}$,$\mathbf{IV_{ABA}}$)** and **TS($\mathbf{III_{ABB}}$,$\mathbf{IV_{ABB}}$)** lie higher in energy with respective barriers of +7.6 kcal and +14.8 kcal/mol. This indicates that the energetically favored route will proceed via $\mathbf{IV_{AAA}}$ and $\mathbf{IV_{AAB}}$ (blue paths Fig. 6).

Up to this this point, the regiochemistry is open. It is decided in the next step by the orientation in which the third alkyne coordinates: in principle, the phenyl group can again be oriented either away from or towards the alkene. It was not possible to optimize the latter. This concurs with an intuitive steric argument given the large size and inflexibility of the phenyl group and the increasingly congested environment around iron. Hence, the respective routes from $\mathbf{IV_{AAA}}$ and $\mathbf{IV_{AAB}}$ to reach the σ-diene, π- alkyne species $\mathbf{V_{AAAB}}$ and $\mathbf{V_{AABB}}$ are precluded (colored red in Fig. 6). The same is true for the previously excluded paths via $\mathbf{IV_{ABA}}$ and $\mathbf{IV_{ABB}}$. This means that the only possible intermediates which would lead to a product with 1,3,5-regiochemistry ($\mathbf{VI_{AABB}}$; $\mathbf{VI_{ABBB}}$) cannot be reached, providing an explanation for the observed regiochemistry solely on thermodynamic grounds.

As a result of the congested environment, the coordination of the final alkyne even in the preferred orientation is uphill. $\mathbf{V_{AAAA}}$ is associated with a computed ΔG value +4.5 kcal/mol above $\mathbf{IV_{AAAA}}$. In $\mathbf{V_{AAAA}}$ the Fe-N_{salen} distance is increased to 3.25 Å; an isomer with a shorter Fe-N bond length of 2.23 Å is higher in energy by 8.7 kcal/mol. This may either indicate that $\mathbf{V_{AAAA}}$ is not stable (dash-dotted line in Fig. 6), or show a second hemilabile mode of the salen ligand. On the adjacent branch, $\mathbf{V_{AABA}}$ has a computed ΔG value +10.4 kcal/mol. Although this is the most uphill intermediate along the route overall, it is still energetically accessible. The next step is the final insertion of an alkyne into the Fe-C bond, forming the coordinated triene $\mathbf{VI_{AAAA}}$ or $\mathbf{VI_{AABA}}$. The ring-closure occurs with concomitant transfer of the H-atom that had originated from the pinacol borane back to the iron. This is consistent with the experimental finding of the DBpin experiment, where the reaction was slower but no deuterated product was found.

At this point, a brief comment on the spin states of the intermediates is in order.[48,49] All species discussed so far had closed-shell electronic structures. For iron, multi-state reactivity must be considered, and so intermediates were optimized with triplet and quintet multiplicities. In some cases,

the higher multiplicity states were energetically accessible or even slightly lower in energy than their closed-shell counterparts (SI, Section 8). For a complete kinetic analysis of the catalysis these states would have to be evaluated. However, the main aim of the mechanistic investigation presented here was to provide a rationale for the observed regioselectivity, which is found to result from steric congestion and thermodynamic accessibility and thereby independent of the spin state.

The resulting catalytic mechanism is shown in Scheme 7A. A molecule of alkyne coordinates into **5** from the forward face of the complex as drawn to get it on-cycle (step A), which is then followed by a hydrometallation by the Fe-H across the alkyne to form an iron vinyl species (step B). This frees the backwards face of the complex for the coordination of another molecule of alkyne in one of two orientations (step C), which is then coordinatively activated so that a rearrangement can occur, producing an iron-bound diene (step D), with the terminal hydrogen of this diene (explicitly drawn) representing the hydrogen which originally formed the iron hydride. This hydrogen atom is oriented towards the iron ion with a H-Fe distance of 2.29 Å. The formation of the diene is followed by the coordination and insertion of a third molecule of alkyne into the Fe-C bond (steps E and F), with the retention of an interaction between the terminal C-H bond and Fe, albeit with an elongation of the H-Fe distance to 2.97 Å. While not hydridic in character in $\mathbf{IV_{AABA}}$, this H atom is poised for transfer back onto the iron ion. A cyclization then occurs to form a coordinated substituted benzene (step G), with the same terminal hydrogen migrating back onto the iron to reform the Fe-H bond. A further molecule of alkyne then coordinates, releasing the product (step H). Overall both computed mechanistic routes shown are concordant with the experimental data and can therefore be considered a plausible description of the catalytic mechanism.

While most substrates tested experimentally preferentially formed 1,2,4-substituted products, there were several which saw much more even splits between 1,2,4- and 1,3,5-substitution patterns. One such substrate was 1-pentyne (**2k**) which afforded a 54:46 ratio between 1,2,4- and 1,3,5-substituted products. The computational results shown in Fig. 6 suggests that the steric limitations on the orientation of the coordinated third alkyne determine whether 1,3,5-substitution is possible. Therefore, it was assessed whether the 1-pentyne equivalents of $\mathbf{V_{AAAB}}$ or $\mathbf{V_{AABB}}$, which are unreachable for **2a**, can be computed, and if so, what the relative thermodynamic position would be.

The results of this study are shown in the bottom panel of Scheme 7. The smaller and more flexible ^{n}Pr groups pendant to the alkyne are more amenable to forming the σ-diene, π-alkyne species with the non-terminal end of the alkyne facing towards the diene (Schemes 7B, 7C). While they are endergonic ($\Delta G(\mathbf{V^{p}_{AAAB}})$=+15.1 kcal/mol, $\Delta G(\mathbf{V^{p}_{AABB}})$= +16.3 kcal/mol), they are in principle accessible as opposed to the **2a** analogues. It was not possible to obtain stable intermediates for $\mathbf{V^{p}_{ABAB}}$ or $\mathbf{V^{p}_{ABBB}}$ as these spontaneously formed their respective σ-triene species (Schemes 7D and 7E). Since it is possible to access more sterically crowded versions of the σ-diene, π-alkyne species (catalysis stage **V**) with 1-pentyne as a substrate, it appears that the route to 1,3,5-regiochemistry is indeed open. This provides an explanation for the less pronounced 1,2,4-regioselectivity for less sterically demanding substrates such as 1-pentyne, 1-heptyne and benzylacetylene. It is interesting to note that, with a handful of exceptions,[23,39] other iron catalyzed (or co-catalyzed) intermolecular cyclotrimerization reactions show the same loss in selectivity for aliphatic substrates. It may be the case that a similar substrate-dictated steric argument as the one made above can be applied to these previous studies.[24,26,50]

Scheme 7. Top panel: Proposed catalytic cycle for the trimerization of 2a using 5 as a starting point. Energies shown are ΔG values (kcal/mol) relative to the previous step of the catalytic cycle (SI- Section 8). The solid blue path from Fig. 6 is shown explicitly, the dashed blue path is also shown. The H atom shown in blue is not incorporated into product, but is integral to catalysis as reflected in KIE data. The third equivalent of 2a is depicted in red to emphasize regioselectivity. Bottom panel: 1-Pentyne regioselectivity tests. Energies expressed as ΔG at 298 K.

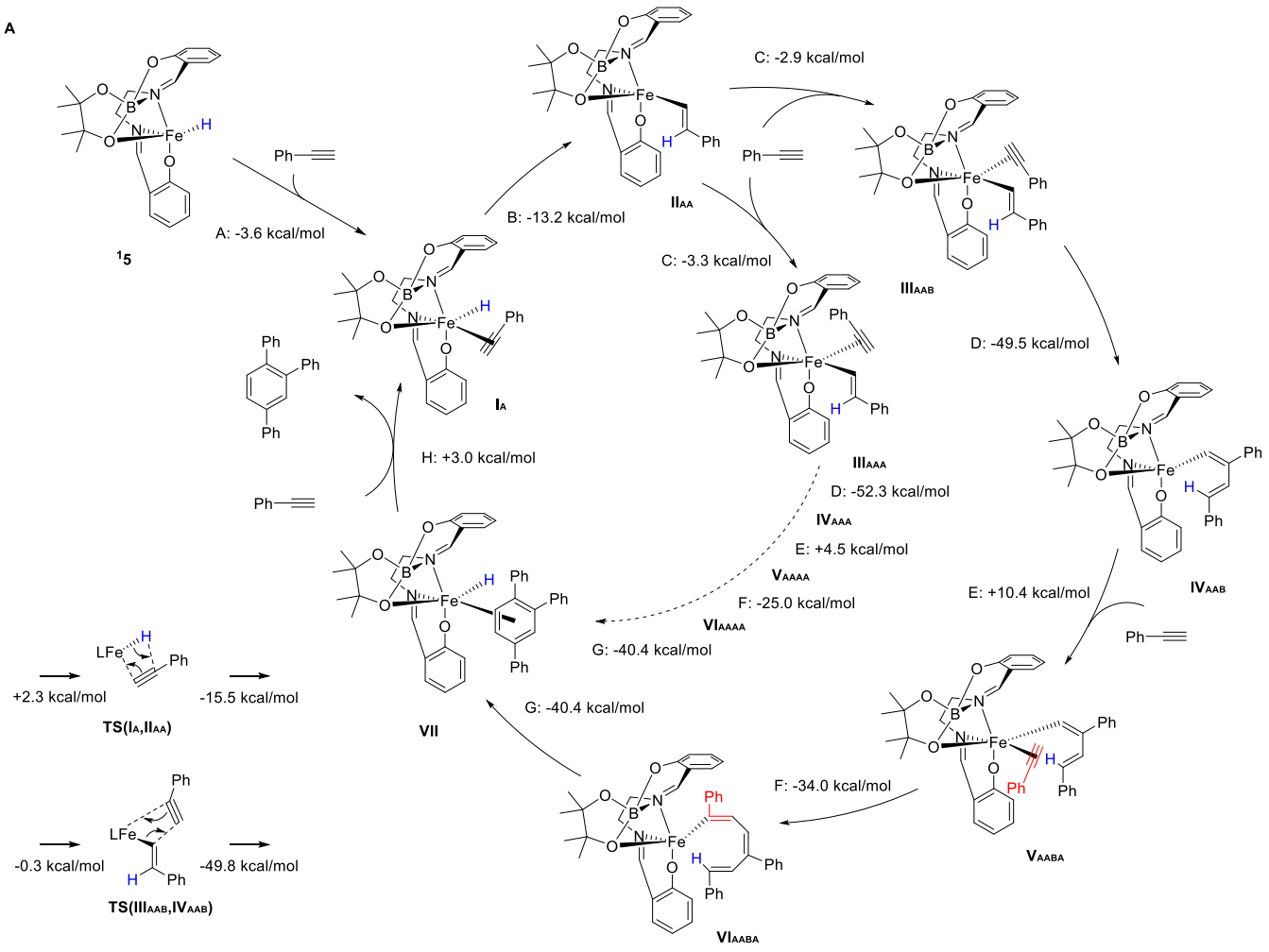

3. CONCLUSION

The alkyne cyclotrimerization presented here shows iron in combination with a cheap and benign tetradentate salen ligand as a powerful catalytic tool mediating a fast C-C bond forming reaction in an atom-efficient and regioselective manner with a wide substrate scope. A number of stoichiometric NMR, X-ray crystallographic, spectroscopic, deuteration, kinetic and complementary computational studies have been performed to elucidate the mechanism by which this catalysis proceeds. These studies provided multiple independent strands of evidence which support catalyst activation proceeding through a combination of [Fe(salen)]$_2$-μ-oxo (**1**) and HBpin to yield an iron hydride complex [Fe(II)H(salen)]·Bpin (**5**) incorporating Bpin through an unprecedented hemilabile mode of the salen ligand. It is shown with density functional theory that the properties of **5** are fully consistent with the experimental observations.

An attempt was made to optimize a more conventional catalytic path using [Fe(salen)] (**4**) alone, which retains the two phenolate oxygens bound to Fe and does not possess a Fe-H. This species proved incapable of catalyzing the cyclotrimerization without HBpin, serving to validate both the computational chemistry methodology and the veracity of the experimental observations supporting it.

The postulated active species **5** appears to possess a highly unusual conformation for Fe-centered salen complexes. To the best of our knowledge, a transition metal salen complex

which undergoes activation of the salen ligand such that a change in coordination number is observed is unique. We show that the observed regioselectivity is intimately connected with the nature of the active species; the intermediates needed for a 1,3,5-substituted product are thermodynamically inaccessible. The proposed catalytic cycle is thus fully consistent with all experimental observations and illuminates a credible rationale for how the regioselectivity of the reaction arises, and why this regioselectivity might break down with smaller and more flexible substrates.

4. METHODS

General method for cyclotrimerization of alkynes

Manipulations were carried out under an argon atmosphere in an M-Braun glove box. **1** (1.7 mg, 0.0025 mmol, 1 mol%), alkyne (0.25 mmol) and pinacolborane (14.5 µl, 0.10 mmol, 40 mol%) were added to a J. Young valve NMR tube. 600 µL of dry MeCN was then added. The sealed reaction was maintained at the required temperature for the time specified for each substrate. The product was isolated by exposing the reaction mixture to air, and adding 1 ml of bench MeCN to quench the remaining pinacolborane. This mixture was then passed through a plug of alumina to remove residual iron and boronic acid. If solid remained in the NMR tube, this was re-dissolved in a minimum of $CHCl_3$ and also passed through the alumina plug. The solvent was removed under a flow of N_2, and the product dried *in vacuo*. $CDCl_3$ was used as the NMR solvent.

ASSOCIATED CONTENT

Supporting Information. This material is available free of charge via the Internet at http://pubs.acs.org." General method for cyclotrimerization of alkynes

AUTHOR INFORMATION

Corresponding Authors

* R.L.Webster@bath.ac.uk
* Krewald@chemie.tu-darmstadt.de

Author Contributions

The manuscript was written through contributions of all authors. All authors have given approval to the final version of the manuscript.

Notes

The authors declare no competing financial interest.

ACKNOWLEDGMENT

We would like to thank the University of Bath for access to the Balena High Performance Computing Service and the Centre for Doctoral Training in Sustainable Chemical Technologies (CSCT, EP/L016354/1) for PhD support (CBPE). CBPE gratefully acknowledges the Royal Society of Chemistry for provision of a Researcher Mobility Grant for a research visit at TU Darmstadt. The EPSRC is thanked for funding (SL, RLW) along with the EPSRC NMSF for mass spectrometry analyses. The Center for Scientific Computing Frankfurt and the Goethe-HLR high performance computing cluster are gratefully acknowledged.

REFERENCES

(1) Kotha, S.; Brahmachary, E.; Lahiri, K. Transition Metal Catalyzed [2+2+2] Cycloaddition and Application in Organic Synthesis. *European J. Org. Chem.* **2005**, No. 22, 4741–4767.

(2) Domínguez, G.; Pérez-Castells, J. Recent Advances in [2+2+2] Cycloaddition Reactions. *Chem. Soc. Rev.* **2011**, *40*, 3430–3444.

(3) Yamamoto, Y. Recent Advances in Intramolecular Alkyne Cyclotrimerization and Its Applications. *Curr. Org. Chem.* **2005**, *9*, 503–519.

(4) Tam-Chang, S. W.; Huang, L. Chromonic Liquid Crystals: Properties and Applications as Functional Materials. *Chem. Commun.* **2008**, No. 17, 1957–1967.

(5) Nielsen, C. B.; Holliday, S.; Chen, H. Y.; Cryer, S. J.; McCulloch, I. Non-Fullerene Electron Acceptors for Use in Organic Solar Cells. *Acc. Chem. Res.* **2015**, *48*, 2803–2812.

(6) Anderson, E. A.; Alexanian, E. J.; Sorensen, E. J. Synthesis of the Furanosteroidal Antibiotic Viridin. *Angew. Chem. Int. Ed.* **2004**, *43*, 1998–2001.

(7) Li, P.; Enche, D. M. Cycloadditions in the Total Synthesis of Sporolide B. *Angew. Chem. Int. Ed.* **2009**, *48*, 5078–5080.

(8) Sripada, L.; Teske, J. A.; Deiters, A. Phenanthridine Synthesis via [2+2+2] Cyclotrimerization Reactions. *Org. Biomol. Chem.* **2008**, *6*, 263–265.

(9) Zou, Y.; Deiters, A. Total Synthesis of Cryptoacetalide. *J. Org. Chem.* **2010**, *75*, 5355–5358.

(10) Kore, A. R.; Yang, B.; Srinivasan, B. Recent Developments in the Synthesis of Substituted Purine Nucleosides and Nucleotides. *Curr. Org. Chem.* **2014**, *18*, 2072–2107.

(11) Ahmad, N. M.; Swarbrick, M. E.; Pryde, D. C.; Ahmad, N. M.; Swarbrick, M. E. Recent Trends and Technologies towards Medicines of the Future. A Joint Meeting of the SMR and the RSC BMCS. London, UK - December 8, 2017. *Drugs Future* **2018**, *43*, 215–224.

(12) Collier, P. N.; Panchagnula, A.; O'Dowd, H.; Le

Tiran, A.; Aronov, A. M. Synthesis of a 6-Aza-Isoindolinone-Based Inhibitor of Phosphoinositide 3-Kinase γ via Ruthenium-Catalyzed [2 + 2 + 2] Cyclotrimerization. *ACS Med. Chem. Lett.* **2019**, *10*, 117–120.

(13) Bertholet, P. E. M. Les Polymers de l'acetylene. *C. R. Hebd. Seances Acad. Sci.* **1866**, *62*, 515–519.

(14) Reppe, W.; Schlichting, O.; Klager, K.; Toepel, T. Cyclisierende Polymerisation von Acetylen I Über Cyclooctatetraen. *Justus Liebigs Ann. Chem.* **1948**, *560*, 104–116.

(15) Schore, N. E. Transition-Metal-Mediated Cycloaddition Reactions of Alkynes in Organic Synthesis. *Chem. Rev.* **1988**, *88*, 1081–1119.

(16) Broere, D.; Ruijter, E. Recent Advances in Transition-Metal-Catalyzed [2+2+2]-Cyclo(Co)Trimerization Reactions. *Synthesis (Stuttg).* **2012**, *44*, 2639–2672.

(17) D'Souza, B. R.; Lane, T. K.; Louie, J. Iron Catalyzed Cycloaddition of Alkynenitriles and Alkynes. *Org. Lett.* **2011**, *13*, 2936–2939.

(18) Nakajima, K.; Takata, S.; Sakata, K.; Nishibayashi, Y. Synthesis of Phosphabenzenes by an Iron-Catalyzed [2+2+2] Cycloaddition Reaction of Diynes with Phosphaalkynes. *Angew. Chem. Int. Ed.* **2015**, *54*, 7597–7601.

(19) Wang, C.; Li, X.; Wu, F.; Wan, B. A Simple and Highly Efficient Iron Catalyst for a [2+2+2] Cycloaddition to Form Pyridines. *Angew. Chem. Int. Ed.* **2011**, *50*, 7162–7166.

(20) Zhang, W.; Loebach, J. L.; Wilson, S. R.; Jacobsen, E. N. Enantioselective Epoxidation of Unfunctionalized Olefins Catalyzed by (Salen)Manganese Complexes. *J. Am. Chem. Soc.* **1990**, *112*, 2801–2803.

(21) Gallagher, K. J.; Webster, R. L. Room Temperature Hydrophosphination Using a Simple Iron Salen Pre-Catalyst. *Chem. Commun.* **2014**, *50*, 12109–12111.

(22) Hilt, G.; Bolze, P.; Harms, K. An Improved Catalyst System for the Iron-Catalyzed Intermodular Ring-Expansion Reactions of Epoxides. *Chem. Eur. J.* **2007**, *13*, 4312–4325.

(23) Brenna, D.; Villa, M.; Gieshoff, T. N.; Fischer, F.; Hapke, M.; Wangelin, A. J. von. Iron-Catalyzed Cyclotrimerization of Terminal Alkynes by Dual Catalyst Activation in the Absence of Reductants. *Angew. Chem. Int. Ed.* **2017**, *56*, 8451–8454.

(24) Neumeier, M.; Chakraborty, U.; Schaarschmidt, D.; O'Shea, V. de la P.; Perez-Ruiz, R.; Wangelin, A. J. von. Photo-Organo-Iron Catalysis for the Cyclotrimerization of Alkynes. *Angew. Chem. Int. Ed.* **2020**.

(25) Karpiniec, S. S.; McGuinness, D. S.; Britovsek, G. J. P.; Patel, J. Acetylene Cyclotrimerization with an Iron(II) Bis(Imino)Pyridine Catalyst. *Organometallics* **2012**, *31*, 3439–3442.

(26) Cheng, J.; Chen, Q.; Leng, X.; Ye, S.; Deng, L. Three-Coordinate Iron(0) Complexes with N-Heterocyclic Carbene and Vinyltrimethylsilane Ligation: Synthesis, Characterization, and Ligand Substitution Reactions. *Inorg. Chem.* **2019**, *58*, 13129–13141.

(27) Gawali, S. S.; Gunanathan, C. Iron-Catalyzed Regioselective Cyclotrimerization of Alkynes to Benzenes. *J. Organomet. Chem.* **2019**, *881*, 139–149.

(28) Spahn, N. A.; Nguyen, M. H.; Renner, J.; Lane, T. K.; Louie, J. Regioselective Iron-Catalyzed [2 + 2 + 2] Cycloaddition Reaction Forming 4,6-Disubstituted 2-Aminopyridines from Terminal Alkynes and Cyanamides. *J. Org. Chem.* **2017**, *82*, 234–242.

(29) Gupta, K. C.; Sutar, A. K. Catalytic Activities of Schiff Base Transition Metal Complexes. *Coord. Chem. Rev.* **2008**, *252*, 1420–1450.

(30) Cozzi, P. G. Metal-Salen Schiff Base Complexes in Catalysis: Practical Aspects. *Chem. Soc. Rev.* **2004**, *33*, 410–421.

(31) *Artificial Metalloenzymes and MetalloDNAzymes in Catalysis: From Design to Applications*; Diéguez, M., Bäckvall, J.-E., Pàmies, O., Eds.; Wiley, 2018.

(32) Erxleben, A. Transition Metal Salen Complexes in Bioinorganic and Medicinal Chemistry. *Inorganica Chim. Acta* **2018**, *472*, 40–57.

(33) Bonadies, J. A.; Maroney, M. J.; Pecoraro, V. L. Structurally Diverse Manganese (III) Schiff Base Complexes: Solution Speciation via Paramagnetic 1H NMR Spectroscopy and Electrochemistry. *Inorg. Chem.* **1989**, *28*, 2044–2051.

(34) Baldwin, M. J.; Gelasco, A.; Pecoraro, V. L. The Effect of Protonation on [Mn(IV)(M2-O)]2 Complexes. *Photosynth. Res.* **1993**, *38*, 303–308.

(35) Feng, X.; Li, S. H.; Sun, Q. Q.; Lei, P. P.; Xie, C. Z. A Propanediamine-Bridged Dinuclear Iron(III) Complex: Synthesis, X-Ray Analyses, Spectral Studies, and Magnetic Properties. *Russ. J. Coord. Chem.* **2011**, *37*, 377–381.

(36) Jia, H. P.; Li, W.; Ju, Z. F.; Zhang, J. Synthesis, Crystal Structure and Magnetic Properties of an Oxalate-Bridged Diiron(III) Complex {[FeIII(Salapn)]2(C2O4)}. *J. Mol. Struct.* **2007**, *833*, 49–52.

(37) Rajender Reddy, K.; Rajasekharan, M. V.; Tuchagues, J. P. Synthesis, Structure, and Magnetic Properties of Mn(Salpn)N3, a Helical Polymer, and Fe(Salpn)N3, a Ferromagnetically Coupled Dimer (SalpnH2 = N,N′-Bis(Salicylidene)-l,3-Diaminopropane). *Inorg. Chem.* **1998**, *37*, 5978–5982.

(38) Romero, E. A.; Peltier, J. L.; Jazzar, R.; Bertrand, G. Catalyst-Free Dehydrocoupling of Amines, Alcohols, and Thiols with Pinacol Borane and 9-Borabicyclononane (9-BBN). *Chem. Commun.* **2016**, *52*, 10563–10565.

(39) Lipschutz, M. I.; Chantarojsiri, T.; Dong, Y.; Tilley, T. D. Synthesis, Characterization, and Alkyne Trimerization Catalysis of a Heteroleptic Two-Coordinate FeI Complex. *J. Am. Chem. Soc.* **2015**, *137*, 6366–6372.

(40) Griller, D.; Ingold, K. U. Free-Radical Clocks. *Acc. Chem. Res.* **1980**, *13*, 317–323.

(41) Sonnenberg, J. F.; Morris, R. H. Distinguishing Homogeneous from Nanoparticle Asymmetric Iron Catalysis. *Catal. Sci. Technol.* **2014**, *4*, 3426–3438.

(42) Widegren, J. A.; Finke, R. G. A Review of the Problem of Distinguishing True Homogeneous Catalysis from Soluble or Other Metal-Particle Heterogeneous Catalysis under Reducing Conditions. *J. Mol. Cat. A.* **2003**, *198*, 317–341.

(43) Chapman, M. R.; Henkelis, S. E.; Kapur, N.; Nguyen, B. N.; Willans, C. E. A Straightforward Electrochemical Approach to Imine- and Amine-Bisphenolate Metal Complexes with Facile Control Over Metal Oxidation State. *ChemistryOpen* **2016**, *5*, 351–356.

(44) Nakazawa, H.; Itazaki, M. Fe–H Complexes in Catalysis. In *Iron Catalysis*; Springer, Berlin, Heidelberg, 2011; pp 27–81.

(45) Bhattacharya, P.; Krause, J. A.; Guan, H. Iron Hydride Complexes Bearing Phosphinite-Based Pincer Ligands: Synthesis, Reactivity, and Catalytic Application in Hydrosilylation Reactions. *Organometallics* **2011**, *30*, 4720–4729.

(46) Daida, E. J.; Peters, J. C. Considering FeII/IV Redox Processes as Mechanistically Relevant to the Catalytic Hydrogenation of Olefins by [PhBPiPr3]Fe-Hx Species. *Inorg. Chem.* **2004**, *43*, 7474–7485.

(47) Halpern, J. Mechanistic Aspects of Homogeneous Catalytic Hydrogenation and Related Processes. *Inorganica Chim. Acta* **1981**, *50*, 11–19.

(48) Schröder, D.; Shaik, S.; Schwarz, H. Two-State Reactivity as a New Concept in Organometallic Chemistry. *Acc. Chem. Res.* **2000**, *33*, 139–145.

(49) Shaik, S.; Hirao, H.; Kumar, D. Reactivity of High-Valent Iron-Oxo Species in Enzymes and Synthetic Reagents: A Tale of Many States. *Acc. Chem. Res.* **2007**, *40*, 532–542.

(50) Bu, X.; Zhang, Z.; Zhou, X. Switching from Dimerization to Cyclotrimerization Selectivity by FeCl3 in the Y[N(TMS)2]3-Catalyzed Transformation of Terminal Alkynes: A New Strategy for Controlling the Selectivity of Organolanthanide-Based Catalysis. *Organometallics* **2010**, *29*, 3530–3534.

Table of Contents Entry

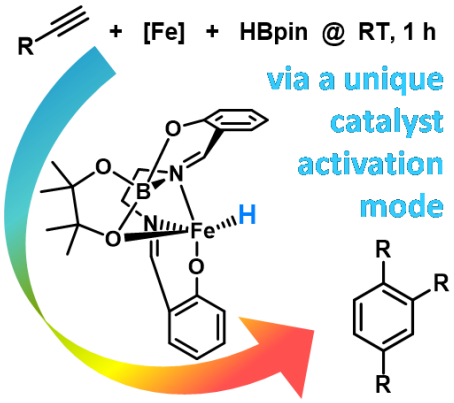
R
+ [Fe] + HBpin @ RT, 1 h
via a unique
catalyst
activation
mode
O
O
B
N
O
N
Fe
H
O
R
R
R

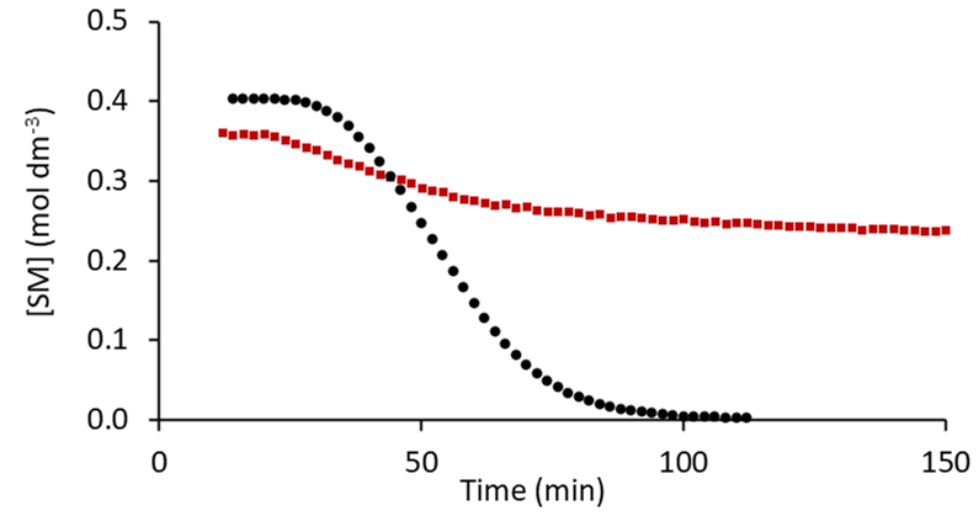

Figure 1. Concentration of 2b (●) over time under standard conditions, and with PMe3 additive (■), calculated by 1H NMR spectroscopy against 1,3,5-trimethoxybenzene (TMB) internal standard.

171x92mm (120 x 120 DPI)

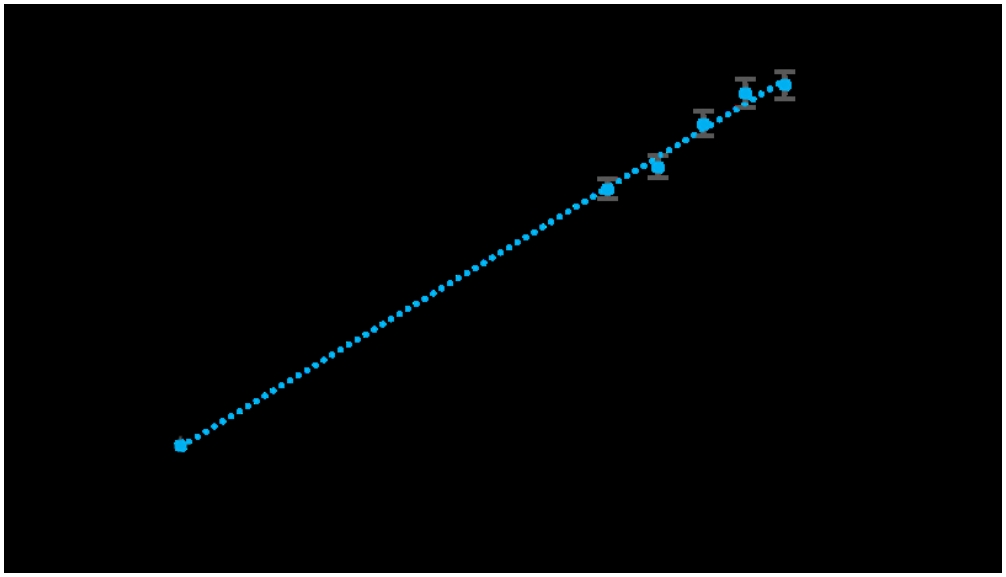

Figure 2. [1]0.5 vs rate. R2 of line through origin > 0.995, therefore reaction 0.5 order with respect to the pre-catalyst.

171x97mm (120 x 120 DPI)

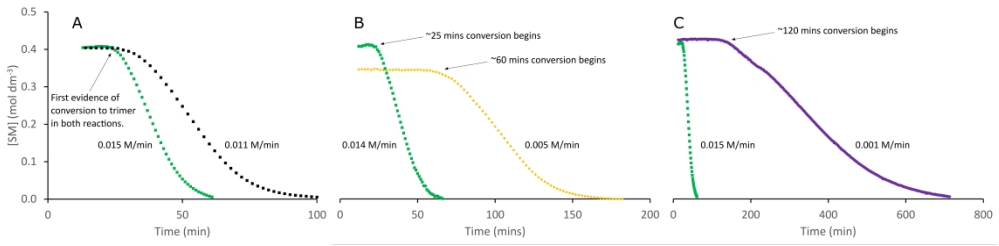

Figure 3. Reaction profiles conducted in CD3CN, quantification by 1H NMR vs. TMB internal standard. A: 2a (■) and 2b (■) trimeri-zations with 1 under standard conditions. B: 2a trimerization with 1 using HBpin (■) and DBpin (◆), both added as 1.35 M solutions in benzene. C: Profile of 2a trimerizations in CD3CN using 6 (●) and 1 (■) as catalysts. Rates shown are for the linear conversion phase of the reactions.

686x166mm (300 x 300 DPI)

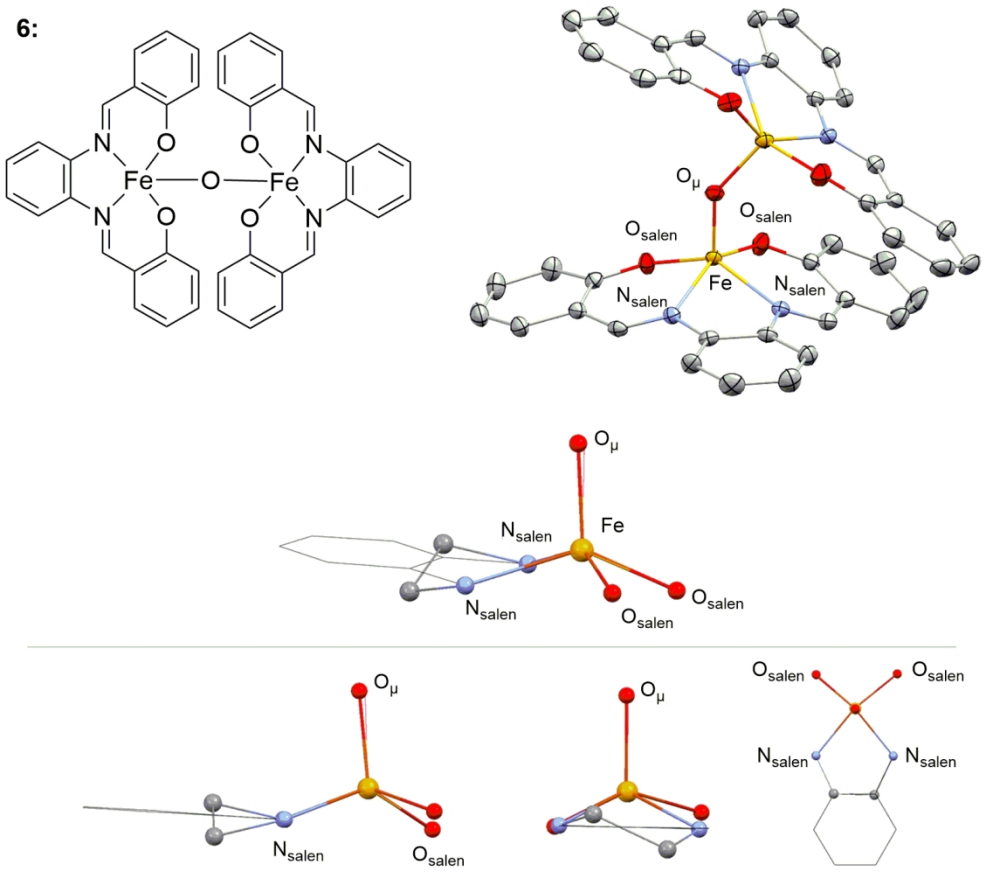

Figure 4. Top: complex 6, with phenyl backbone, planar nature of ligand shown in crystal structure. Bottom: wireframe of 6 overlaid with 1 shown along different axes to demonstrate the planarity of 6.

137x130mm (300 x 300 DPI)

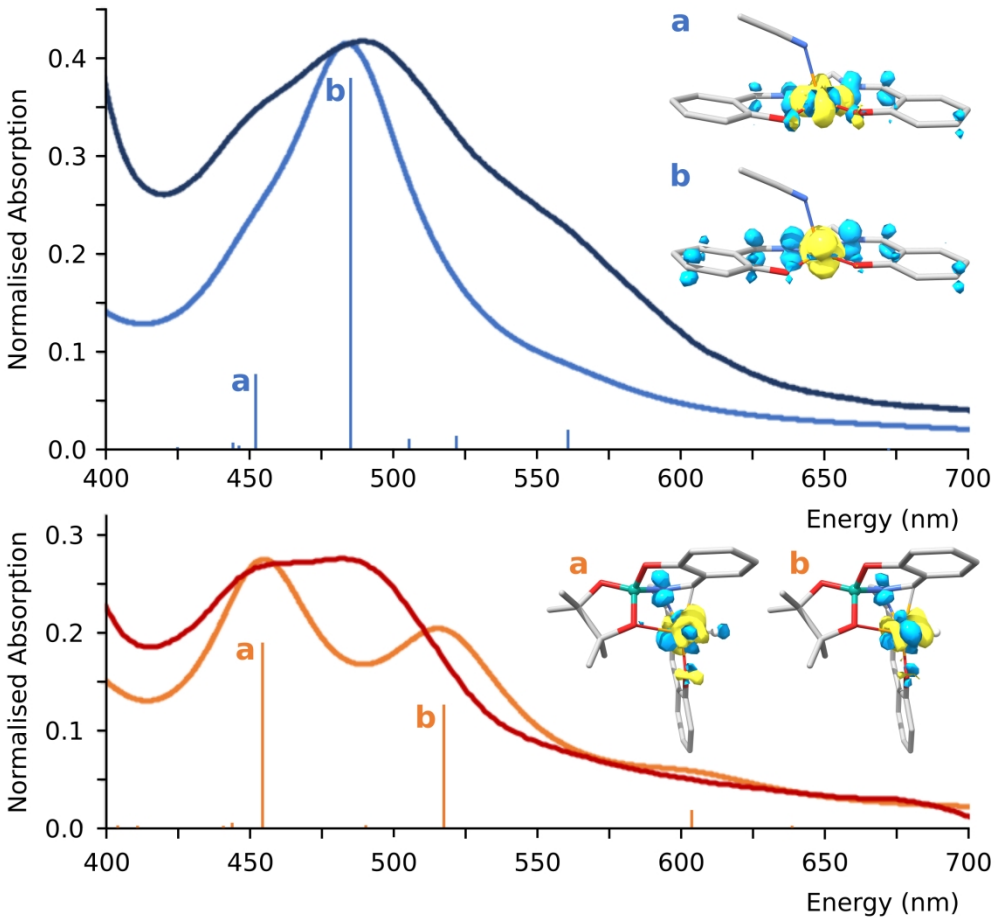

Figure 5. Top: UV-Vis spectra of 4 in MeCN (experiment: dark blue, calculation: light blue). Bottom: experimental spectrum of 1 + 10 eq. HBpin after 20 min (red trace, maxima at 452 and 490 nm) and predicted UV-Vis spectrum of 5 (orange trace, maxima at 455 and 517 nm). Vertical lines show individual cal-culated transitions which are broadened to obtain the line spectra; intensities of the calculated spectra are scaled to the maxima of the experimental spectra. The insets show the dif-ference densities associated with the most intense transitions (yellow: density loss; light blue: density gain; contour value: 0.0035).
2.4

83x76mm (800 x 800 DPI)

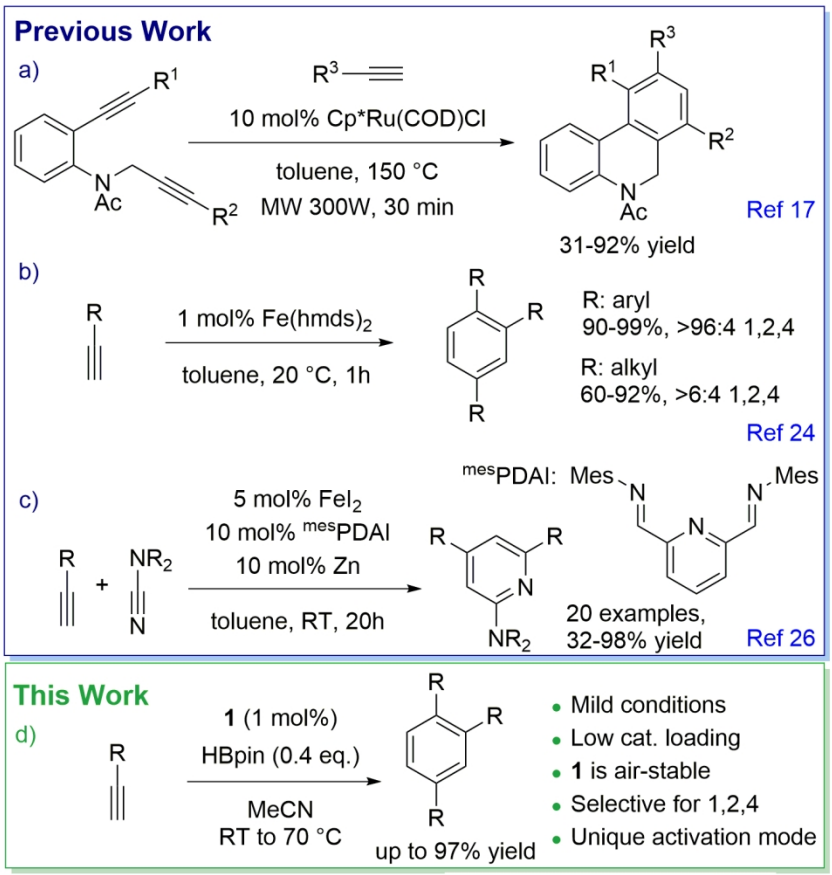

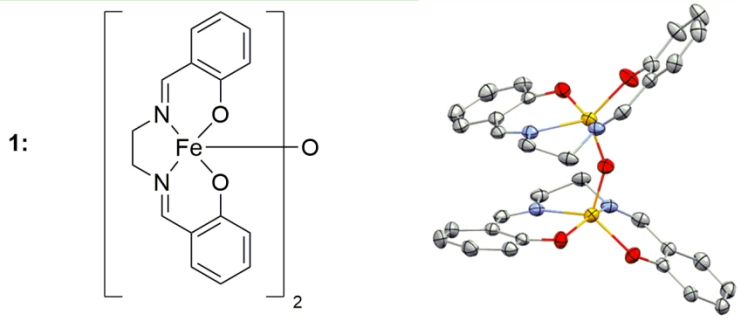

125x179mm (300 x 300 DPI)

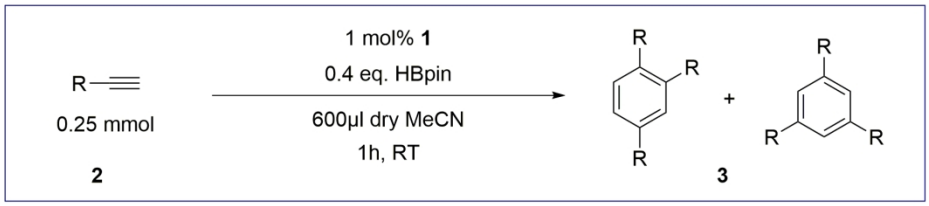

Spectroscopic Purity % [Isolated yield %] Isomeric ratio 1,2,4 : 1,3,5

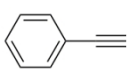

3a: 100 [97] 98:2

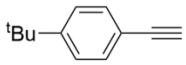

3b: 100 [65] 100:0[a]

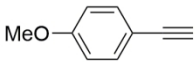

3c: 97[70] 91:9

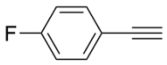

3d: 100 [90] 98:2

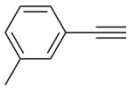

3e: 98 [87] 95:5

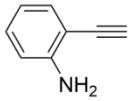

3f: 100 [42] 100:0[b]

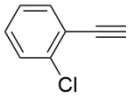

3g: 100 [81] 95:5

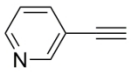

3h: 100 [16] 100:0[c]

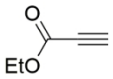

3i: 100 [81] 95:5

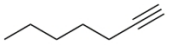

3j: 100 [72] 54:46[c]

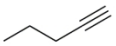

3k: 87 [8] 54:46

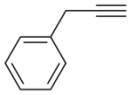

3l: 67 [4] 67:33

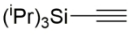

3m: Int. mixture[d]

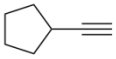

3n: NR[c]

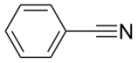

3o: NR

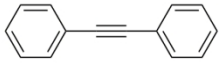

3p: Int. mixture[d]

167x152mm (300 x 300 DPI)

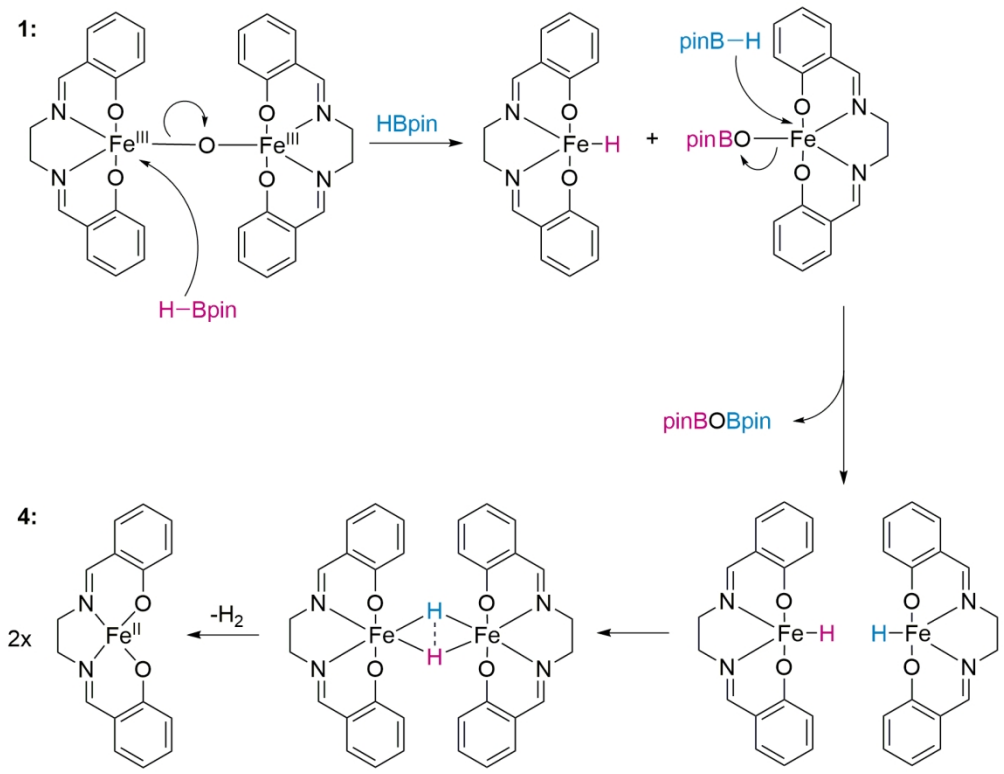

154x118mm (300 x 300 DPI)

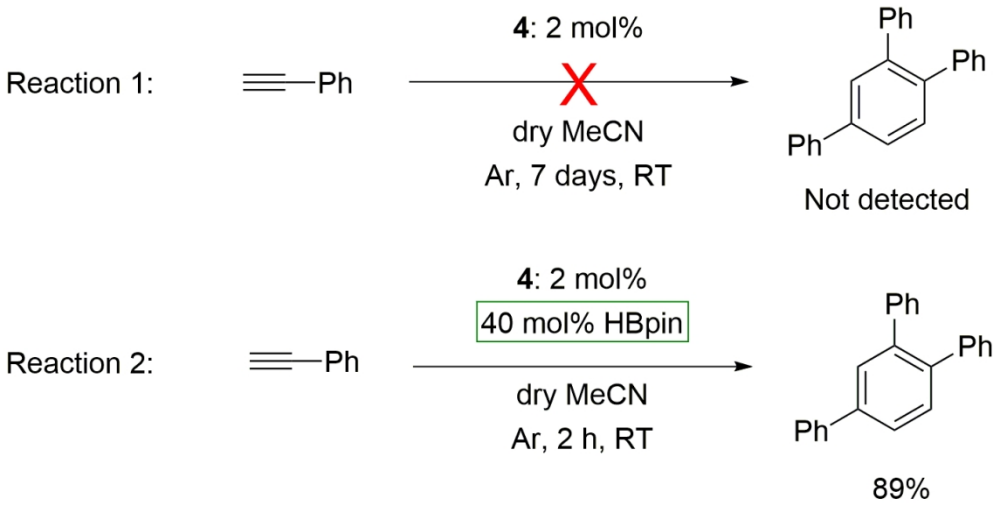

120x61mm (300 x 300 DPI)

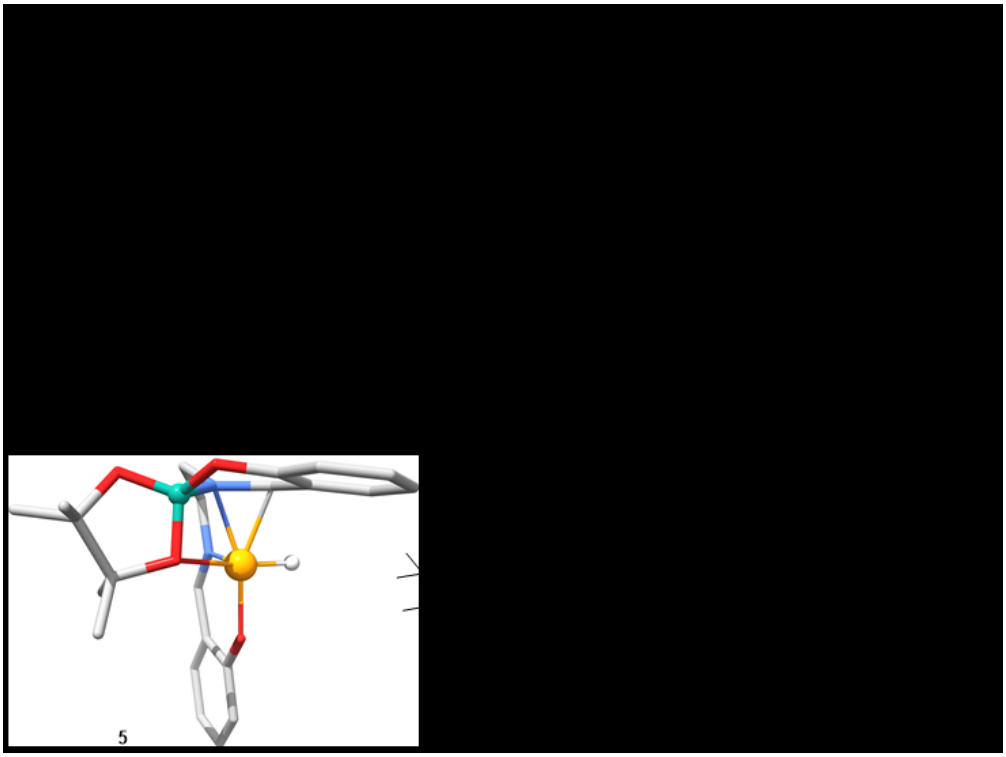

155x116mm (120 x 120 DPI)

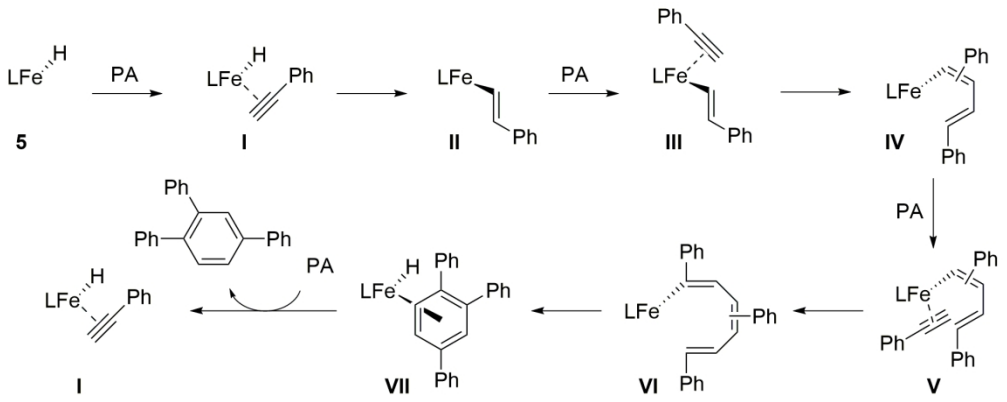

169x68mm (300 x 300 DPI)

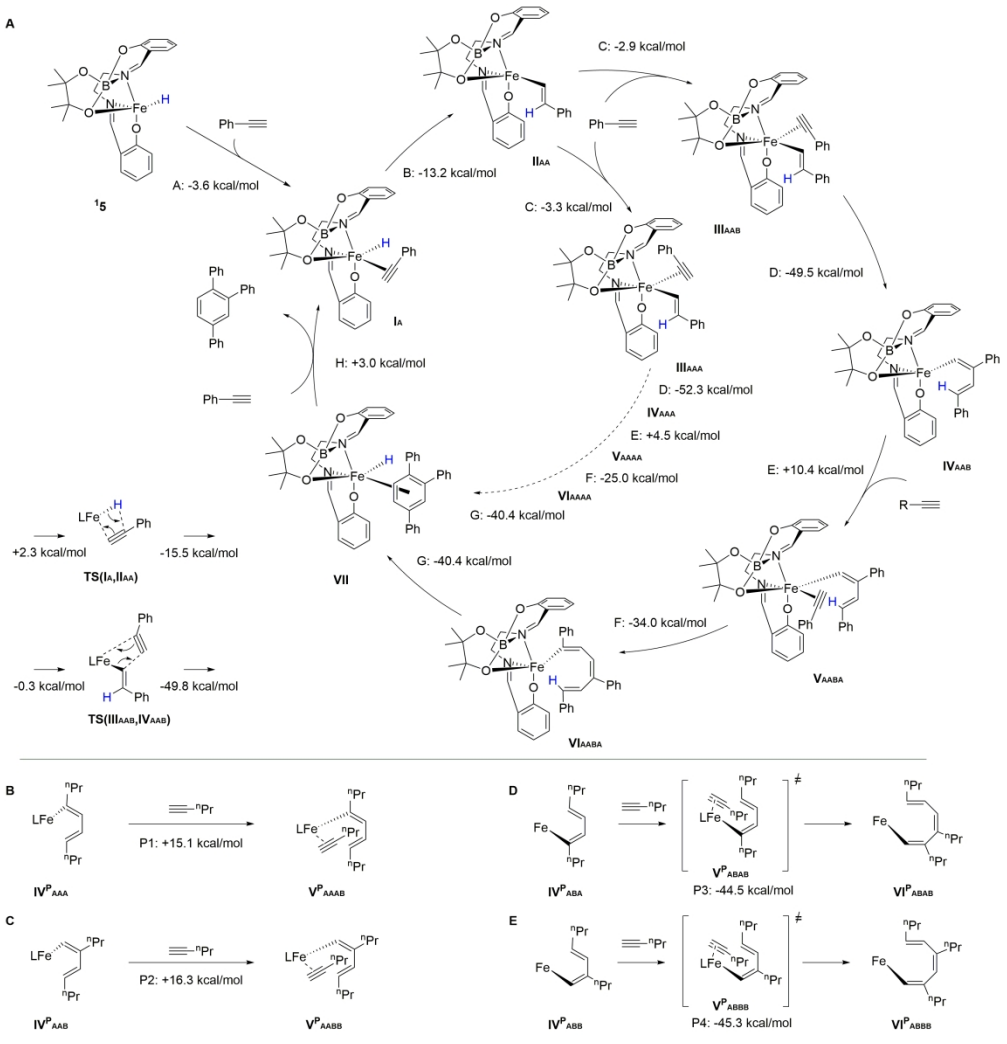

281x290mm (300 x 300 DPI)

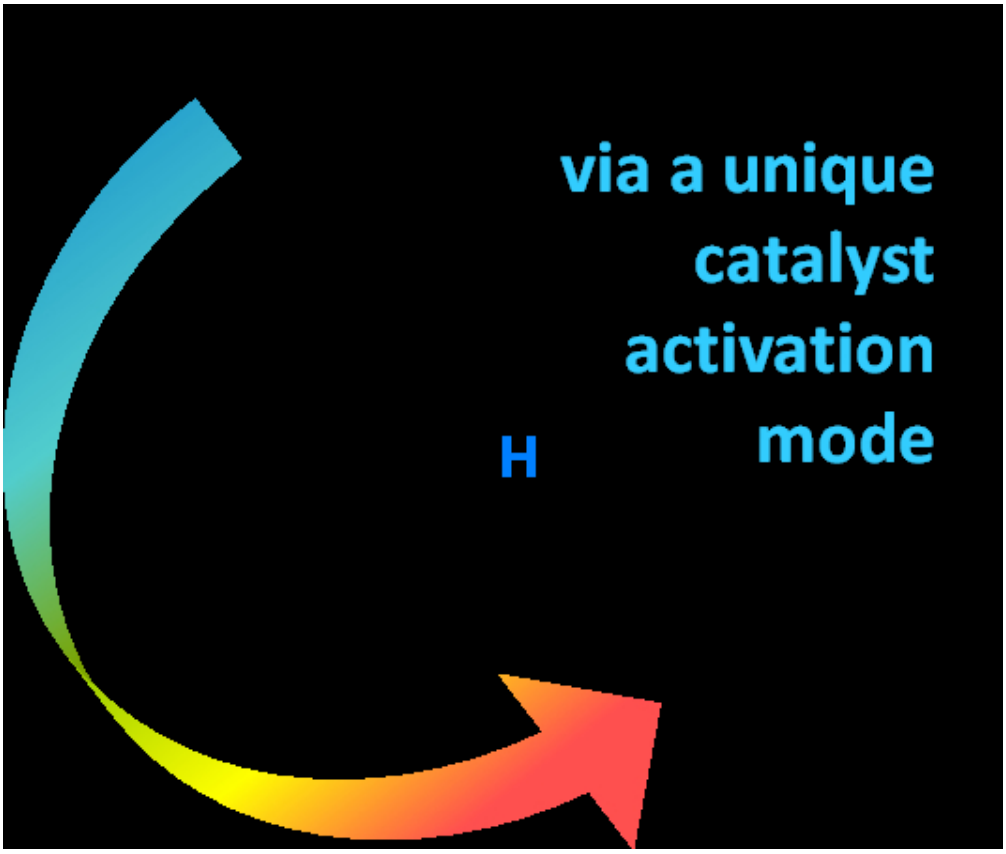

112x95mm (120 x 120 DPI)